



Spray Coating Experiments: Setups and Methodologies



**The latest eBook from
Advanced Optical Metrology.
Download for free.**

Spray Coating Experiments: Setups and Methodologies, is the third in our Thin Films eBook series. This publication provides an introduction to spray coating, three article digests from Wiley Online Library and the latest news about Evident's Image of the Year Award 2022.

Wiley in collaboration with Evident, are committed to bridging the gap between fundamental research and industrial applications in the field of optical metrology. We strive to do this by collecting and organizing existing information, making it more accessible and useful for researchers and practitioners alike.

EVIDENT
OLYMPUS

WILEY

Hierarchically Nanostructured Janus Membranes Toward Sustainable and Efficient Solar-to-Thermal Management

Shan Li, Peng Xiao,* Weiqing Yang, Chang Zhang, Jincui Gu, Shiao-Wei Kuo, and Tao Chen*


Solar-enabled thermal management is emerging as a promising candidate to exploit green, low-cost and efficient heat-related applications, which has drawn extensive intensity for the development of solar-to-thermal materials with high-performance and desirable functionality. However, there still remain considerable challenges, such as the sharp temperature fluctuations under water-related environment, high cost, complex fabrication approaches and limited energy efficiency. Here, superhydrophobic and photothermal nanostructured Janus membranes composed of hierarchical candle soot and transparent polydimethylsiloxane is proposed in a simple, low-cost, and effective way. The achieved membranes can readily adapt to curved surfaces and enable efficient solar-to-thermal capability of ≈ 68 °C under 1 sun and good water-repellant property of ≈ 159.7 . Therefore, it can still maintain stable temperature without remarkable temperature decline when exposed to the high-moisture environment. Also, the asymmetric structure can further endow the membrane with declined heat dissipation for high-performance thermal management. Moreover, it can further function as a self-supported agricultural film to continuously heat the soils with stable temperature for efficient bean growth, demonstrating significant potential in the new generation of urban agriculture.

S. Li, P. Xiao, W. Yang, C. Zhang, J. Gu, T. Chen
Key Laboratory of Marine Materials and Related Technologies
Zhejiang Key Laboratory of Marine
Materials and Protective Technologies
Ningbo Institute of Materials Technology and Engineering
Chinese Academy of Sciences
Ningbo 315201, China
E-mail: xiaopeng@nimte.ac.cn; tao.chen@nimte.ac.cn

S. Li, P. Xiao, W. Yang, C. Zhang, J. Gu, T. Chen
Qianwan Institute of CNITECH
Zhongchuang 1st Road
Zhongchuang Park
Hangzhou Bay New Zone
Ningbo, Zhejiang 315336, China

S. Li, P. Xiao, W. Yang, C. Zhang, J. Gu, T. Chen
School of Chemical Sciences
University of Chinese Academy of Sciences
19A Yuquan Road, Beijing 100049, China

S.-W. Kuo
Department of Material and Optoelectronic Science
Center of Crystal Research
National Sun Yat-Sen University
Kaohsiung, Taiwan 804, China

 The ORCID identification number(s) for the author(s) of this article can be found under <https://doi.org/10.1002/adfm.202209654>.

DOI: 10.1002/adfm.202209654

1. Introduction

Nowadays, some extreme climates such as strong cold air that seriously threaten the public health and crop growth has occurred frequently with global warming.^[1–5] A typical example of cold wave caused by La Niña phenomenon can not only frostbite people, but severely delay the germination and the sowing of crops, which may lead to massive losses to social economy, resources and environment.^[6–8] Since diverse heaters are alternatively implemented to elevate the temperature, there are some concerns of economy and ecological environment, such as the huge consumption of fossil fuels or power energy.^[9–14] Besides, the latest statistics shows that $\approx 68\%$ of the world's population is estimated to be in urban areas by 2050, leading to diminishing agricultural lands, heavy burden on food supplies and limited energy.^[15–17] Alternatively, the development of urban agriculture targeted as high-efficient utilization of resource is

expected to be a promising solution.^[18–20] Therefore, the exploitation of eco-friendly, low-energy, and renewable heating technologies has aroused widespread concern.

Solar energy is regarded as an ideal resource with renewable, environmentally friendly and cost-free features. Based on these advantages, significant advances have been dedicated to develop a series of photothermal and photovoltaic systems and related devices.^[21–26] In particular, the solar-to-thermal conversion is a direct, simple and efficient way to convert solar energy input to considerable heat. The past years have witnessed the rapid development of photothermal materials owing to their great importance in many scenarios, such as indoor energy efficient cooling/heating,^[27,28] personal thermal management,^[29,30] efficient solar water evaporation,^[31] desalination,^[32] energy/heat storage,^[33,34] and thermal camouflage.^[35,36] Especially in the field of heat management, storage and energy reuse, efficient photothermal conversion materials play a crucial role in the management and utilization efficiency of thermal energy. At present, typical examples of intrinsic materials can efficiently convert solar energy to considerable heat, such as metal nanoparticles,^[37] carbon nanomaterials,^[33,38–40] graphene nanosheets,^[41,42] Mxene nanosheets,^[43,44] conjugated polymers,^[45,46] etc. Particularly, the well-designed construction of macroscopic nano- or

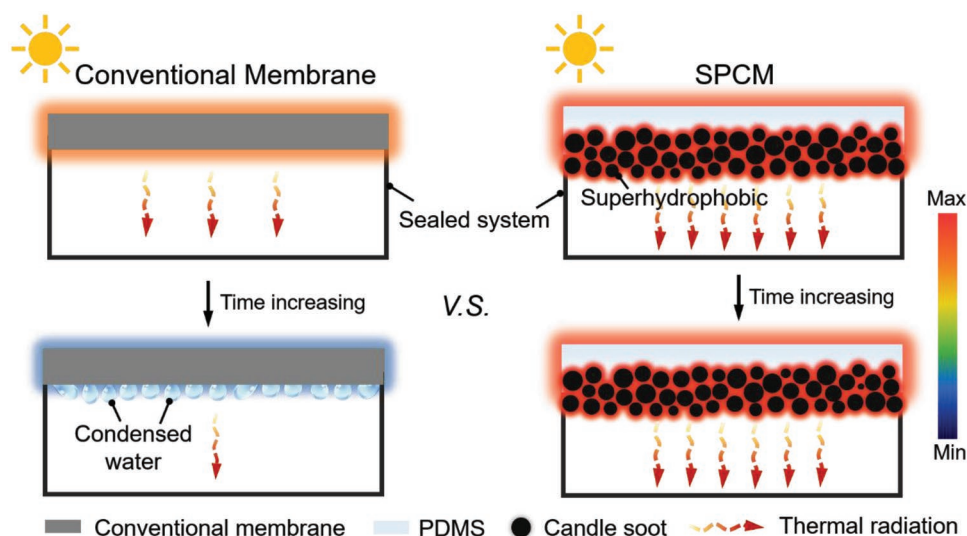
micro-structures into above systems can further efficiently strengthen the photothermal performance.^[27,47–50] Therefore, a variety of thermal management materials have been developed by researchers, such as photothermal film,^[51] photothermal fiber,^[52] photothermal coating,^[53] semiconductor photothermal material^[54] and photothermal phase-changing hydrogels^[34] to achieve multi-scene and multi-functional applications. Zhou et al. developed a light-adaptive shutter inspired by Mimosa, which can switch on and off according to the fluctuation of the solar illumination, and realize the indoor temperature stability and heat storage throughout the day.^[33] In addition, Wu et al. reported a temperature adaptive radiation coating, which can automatically reduce the emissivity from 0.9 (higher than 30 °C) to 0.2 when the ambient temperature is lower than 15 °C, further realizing all-season household thermal regulation.^[27]

However, when exposed to the environment of liquid water or even high moisture, most of the conventional photothermal systems may inevitably experience sharp decline of generated temperature due to the high specific heat of water, resulting in noncontinuous heating performance. In addition, the condensed water droplets not only damage crops but also freeze and crack the membrane system in cold weather, which greatly limits the application of conventional photothermal systems (Scheme 1). Therefore, it is highly preferable to introduce superhydrophobic strategy into photothermal materials aim to pursue targeted materials with water-resistant, cost-effective, high-efficient, and expandable features.^[55,56]

Recently, common, cheap, easy to manufacture, and high photothermal efficiency (absorption rate: ≈100%) of candle soot has attracted extensive attention of researchers.^[57,58] He et al. reported the super-hydrophobic multistage structure by simply burning a layer of raw candle soot on the glass sheet (CS). In order to enhance the CS layer, a layer of the hydrophobic polymer was deposited to obtain a super-hydrophobic photothermal ice-resistant surface.^[48] The simple and readily available nanoscale super-hydrophobic hierarchical structure

of candle soot can not only trap sunlight in the hierarchical structure, but also enhance light absorption to achieve high photothermal efficiency. Moreover, candle soot also can prevent condensation of water vapor and keep the surface dry to reduce heat loss. Therefore, low price, simple, environmental protection, energy-saving candle soot has a wide application prospect in the field of new photothermal materials for urban agriculture.

Herein, we have designed hierarchically nanostructured Janus membranes with candle soot partially embedded into the transparent and thin elastomer matrix (Figure 1a), obtained a Janus composite membrane with a robust interlocked structure. The obtained interlocked structure ensures high emissivity for effective IR irradiation of the membrane and robust surface of superhydrophobic photothermal surface. Through a typical burning procedure, large-area candle soot with hierarchically nanostructures can be readily acquired. Followed by adhesive transfer of the partial cross-linking polydimethylsiloxane (PDMS) elastomer fabricated on water surface and secondary curing, the superhydrophobic, photothermal candle soot membrane (SPCM) can be successfully achieved, which enables enhanced capability of solar-to-thermal conversion of ≈68 °C under 1 sun and favorable superhydrophobic feature of ≈159.7°. Moreover, the asymmetric structure of the membrane can effectively weaken the heat dissipation with the PDMS side as the outer layer of light transmission and thermal isolation. Therefore, the membrane has the potential to be used as featured thermal management device. When integrated in a closed system under solar irradiation, the membrane can resist the condensation of water and continuously generate considerable heat even under the condition of high moisture, achieving a stable thermal management in greenhouse system. Furthermore, as a demo, it can be also used as a heating and lightproof membrane to efficiently provide suitable and stable temperature for bean sprouts. Compared with the commercial PVC system, the germination rate of the SPCM system could



Scheme 1. Structure and working principle of SPCM and conventional membrane. With the increase of illumination time, the temperature and photothermal efficiency of conventional membrane decrease due to the condensation of water droplets. On the contrary, benefitting by the superhydrophobic properties of SPCM, SPCM resist the condensation of water and continuously generate considerable heat even under the condition of high moisture.

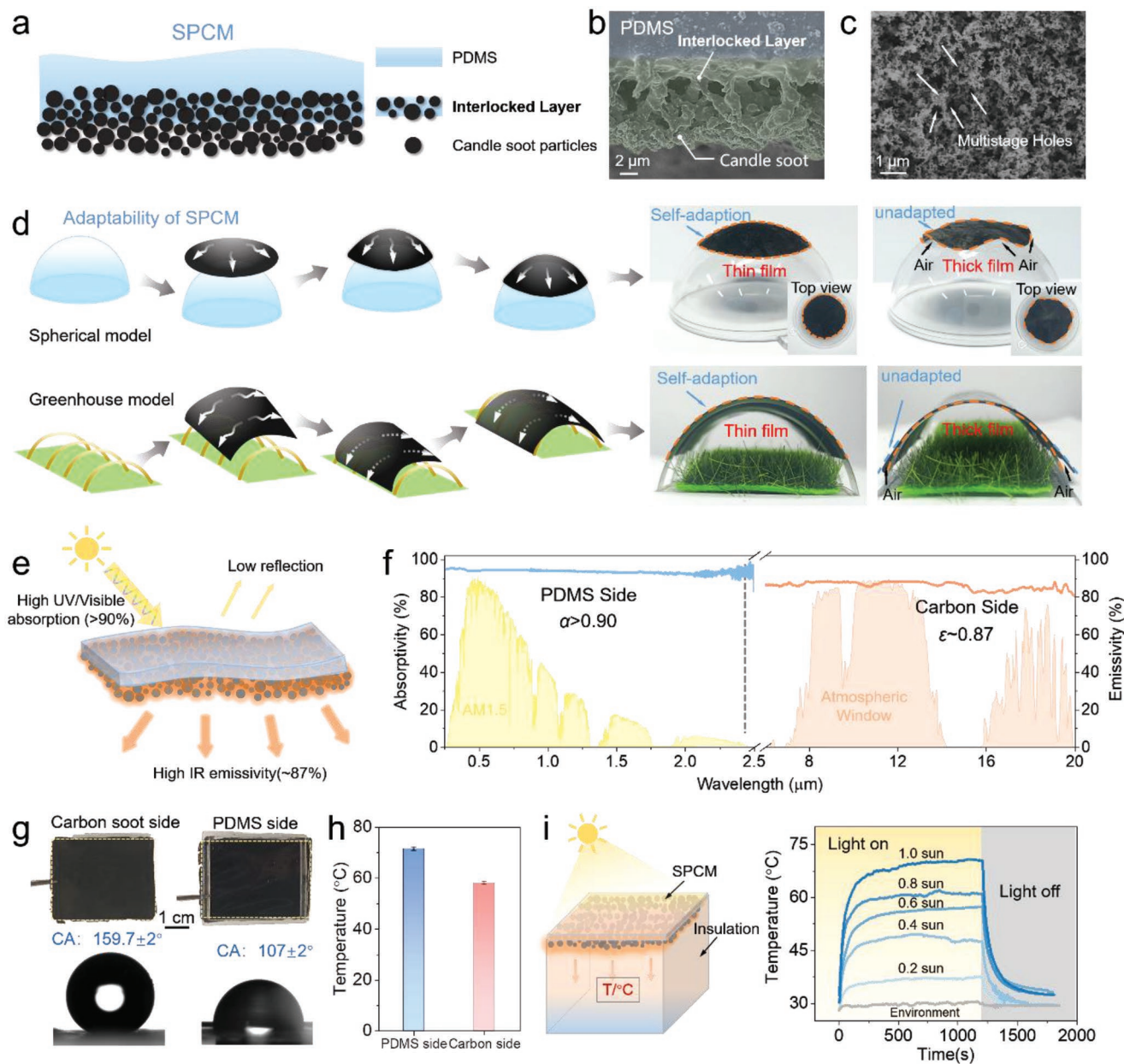


Figure 1. Characteristics and performance of SPCM. a) Schematic diagram of SPCM with interlocked layer structure. b) SEM images of SPCM with outstanding interlocking layers by prepared at water/air interface. c) SEM image of multistage pores structure on SPCM surface. d) Adaptive images of thin ($\approx 50 \mu\text{m}$) and thick ($\approx 150 \mu\text{m}$) SPCM surfaces in hemispheres and greenhouse models. e) Working mechanism diagram of SPCM. f) SPCM with high-efficiency solar absorptivity on the PDMS side and excellent thermal emissivity on the carbon side during heating (α is sunlight absorptivity, ϵ is IR emissivity). g) Optical photographs and wettability of SPCM on both sides (the sample size: $\approx 4 \text{ cm} \times 3 \text{ cm}$, test number: $n = 2$, CA: contact angle, three different positions were measured for each sample, water droplets = $3 \mu\text{L}$). h) The temperature on the PDMS and carbon sides of the SPCM measured by thermocouple. i) Schematic diagram of thermal management model and temperature-time curve of SPCM thermal management under different sunlight (the sample size: $\approx 3 \text{ cm} \times 3 \text{ cm}$, $1 \text{ sun} = 1000 \text{ W m}^{-2}$).

be increased by $\approx 30\%$, demonstrating a promising potential in the new-generation urban agricultural system.

2. Results and Discussion

The typical fabrication strategy of Janus membrane was schematically displayed in Figure S1 (Supporting Information), in

which the candle soot was first deposited on the glass substrate. To achieve a stable interlocked interface, a partially cross-linked PDMS was fabricated on water surface to realize favorable adhesive and easily transferrable features. By direct contact between candle soot and PDMS from the air side and subsequent complete curing procedure, the SPCM could be successfully achieved, which could be easily peeled off from the glass substrate. Note that the specific precure time was considered

to be an important factor for the formation of uniform composite. As shown in Figure S2 (Supporting Information), prior to 30 min, PDMS layer on water surface was flowable and only part of the PDMS could be transferred onto candle soot surface, resulting in visible damage on the resulted SPCM. When the curing time ranged from 40 to 50 min, the PDMS membrane in a semi-polymerized state was formed. As a result, a homogeneous SPCM with interlocked structural interface could be fabricated. Further increasing the curing time of ≈ 80 min enabled a complete curing PDMS membrane. What's more, the influence of water temperature (25 °C, 65 °C, 95 °C) and vacuum during the process of uniform composite of SPCM was also explored. As shown in Figures S3,S4a (Supporting Information), it is easy to observe that the complete homogeneous membrane can be obtained at 65 °C and the SPCM is difficult to be obtained completely and uniformly at both low and high temperatures. Moreover, it is not difficult to conclude that vacuum has no effect on the uniformity of the SPCM (Figure S4b, Supporting Information). However, it was observed that candle soot without interlocked interface was mostly exposed to the air side, leading to undesirable mechanical instability (Figure S5, Supporting Information). Based on above consideration, we have adopted the factor of PDMS precure time of 45 min in our system. In addition, the interface strategy can enable controlled membrane thickness with high uniformity. As displayed in Figure S6 (Supporting Information), a series of thickness of SPCM (24, 48, 58, and 68 μm) was fabricated using different PDMS mass (2, 3, 3.5, and 4 g).

Typically, the transparent and heat-insulated PDMS membrane with thin thickness is characteristic of low light absorption (lower than 1% of the absorptivity) ranging from 200 to 2500 nm, and the photothermal layer of candle soot demonstrates high emissivity of close to 100%) (Figure S7, Supporting Information). The asymmetric interface integration of these two functional parts are considered to be a promising alternative for high-efficient thermal management. For PDMS layer, there is a typical trade-off between transparency (negative correlation with thickness) and heat dissipation (negative with thickness). Therefore, the light absorption of SPCM with different PDMS thickness was conducted via UV-vis absorption spectra to acquire an optimized thickness of PDMS. As shown in Figure S8 (Supporting Information), the total light absorption experienced a negative relationship with the thickness. This is due to the fact that the increase in thickness causes the light to be reflected and dissipated in the propagation path, thus the light absorption by the carbon soot side is correspondingly reduced (Figure S9, Supporting Information). Specifically, compared with the light absorption value of SPCM (28 μm), there was only a slight decrease of that of SPCM with the thickness of 48 μm . Moreover, considering the potential weakened heat insulation of ultrathin membrane, SPCM with the thickness of 48 μm was selected in our system. In addition, the solar-to-thermal conversion of SPCM with a series of thickness was also applied under 0.6 sun (Figure S10, Supporting Information). The result showed that there was a negative correlation between the generated temperature and the thickness of PDMS. However, it was observed that SPCM with the thickness of 48 μm still remained a relatively high temperature. Besides, the photothermal layer of the SPCM was also adjusted by

controlling the burning time. With the increase of the deposition time of the candle soot ranging from 30 s to 5 min, the generated temperature under 1 sun can still maintain a relatively stable value (Figure S11, Supporting Information). However, the resulted emissivity of SPCM increases with the increase of deposition time. And considering the fabrication efficiency and almost stable emissivity, SPCM with burning time of 5 min was alternatively adopted in our system (Figure S12, Supporting Information).

The interlocked structure is expected to provide favorable stability of SPCM. To further characterize the morphology, scanning electron microscopy (SEM) was used to investigate the surface and cross-section information. As shown in Figure 1b, a robust interlocked layer was successfully formed between PDMS and candle soot. The roughness and wettability before and after interlocking layer formation are shown in Figures S13–S15 (Supporting Information). Compared with pure PDMS (without interlocked layer), the superhydrophobicity and roughness of SPCM after crosslinking are significantly increased. The hierarchical pore structure could be also observed. The surface morphology of candle soot further evidenced the formation of hierarchical structures (Figure 1c). Moreover, the stress-strain curve of four films with and without interlocked structure were explored in Figure S16 (Supporting Information). It can be clearly observed that the SPCM demonstrated good mechanical strength for further thermal management applications. In addition, commercial scotch tape was also used to explore the mechanical stability of the SPCM. As shown in Figure S17 (Supporting Information), compared with the control sample (no interlocked interface), there was almost no candle soot residue on the tape surface. Also, the mechanical abrasion resistance of the SPCM was also considered. Benefitted from the fused connection between PDMS and carbon soot, SPCM surface represented favorable mechanical stability under abrasive paper (P600) with 200 g weight applied (Figure S18a,b, Supporting Information). Note that even the SPCM is a slight damaged, the SPCM can still present a good superhydrophobic feature with a contact angle of 152.2° and possess a stable water repellency under 10 cycles of abrasive paper friction. (Figure S18c,d, Supporting Information). More importantly, SPCM with interlocked structure also displayed outstanding ability to convert light into heat between four films (Figure S19, Supporting Information). In a word, the interlocked structure endows the SPCM with stable superhydrophobic and photothermal properties. Owing to the ultrathin feature of the SPCM, it could highly adapt to diverse non-planar surfaces (e.g., circular roof, hollow curved surface) (Figure 1d). To further explore the mechanical properties of SPCM, the film was stretched up to 1000 cycles under 50% strain (Figure S20a,b, Supporting Information). It was found that the surface structure of SPCM was not destroyed even after 1000 tensile tests (Figure S20c,d, Supporting Information). Moreover, the photothermal conversion performance of SPCM was also measured. As shown in Figure S20e (Supporting Information), the temperature-time curve of the film after 1000 stretching cycles is consistent with the original state. Therefore, the superhydrophobic photothermal film is endowed with robust surface structure and stable capability of thermal management. Superior to the conventional thick

membranes, SPCM showed a seamless and adaptive spreading behavior.

More importantly, the asymmetric structure of SPCM could effectively reduce the heat dissipation for high-performance thermal management. Quantificationally, the total energy absorbed by SPCM is in balance with the total energy dissipated. When it reaches steady state,

$$\alpha Q_{\text{sun}} = Q_{\text{rad}} + Q_{\text{conv}} + Q_{\text{cond}} \quad (1)$$

where Q_{rad} , Q_{conv} and Q_{cond} are the heat loss due to thermal radiation, convection, and conduction, respectively. Q_{sun} is the solar illumination power, and α is the sunlight absorptivity of the SPCM. The thermal radiation of SPCM can be interpreted as:

$$Q_{\text{rad}} = Q_{\text{rad,c}} - Q_{\text{E}} \quad (2)$$

$Q_{\text{rad,c}}$ is the thermal radiation energy emitted by SPCM to outer space, which is proportional to emittance ε . Q_{atm} is the absorbed power due to the radiation of ambient air. When the SPCM works, a great amount of emission power from the SPCM directly passes through the atmospheric window at the wavelength range of 8 to 14 μm (where Q_{atm} is around zero), leading to a much higher radiative heat. For indoor thermal management objectives, high thermal emissivity ε and low reflectivity r ($\varepsilon = 1 - r$, film opacity to sunlight) are critical for space heating. The high solar absorptivity α significantly improves the heating capacity. This advantage of SPCM based on asymmetric structure enables efficient use of energy.

The solar absorption and emissivity of the SPCM was measured using Fourier Transform Infrared (FTIR) and UV-vis-NIR spectroscopy with an integrating sphere. As shown in Figure 1e,f, the PDMS side of SPCM showed high absorption rate of >90% and low reflectance (Figure S21, Supporting Information), and the carbon side represented high thermal emissivity of $\approx 87\%$. Due to the composite of candle soot and PDMS, the emissivity of SPCM decreased compared to pure candle soot (≈ 1). Benefitted from the hierarchical structure of the candle soot, the SPCM demonstrated a good superhydrophobic feature with water contact angle (WCA) of $\approx 159.7^\circ$, which could endure the unfavorable condensation of water droplets to maintain stable temperature (Figure 1g). Owing to the asymmetric structural distribution of carbon particles in PDMS, the mechanical property of SPCM cannot be significantly affected. As shown in Figure S22 (Supporting Information), with the increase of carbon particles, the mechanical strength of the asymmetric superhydrophobic photothermal film experience a slight change. Specifically, it was found that the temperature on the PDMS side of the SPCM was $\approx 71.4^\circ\text{C}$, which was higher than that of the candle soot side (Figure 1h). Infrared thermal images also shows that the temperature on both sides of SPCM is consistent with the trend of the thermocouple measurement results (Figure S23, Supporting Information). This phenomenon may derive from the potential thermal accumulation effect due to the good thermal barrier of PDMS layer. Therefore, SPCM was preferred to function as solar-enabled heater with the PDMS layer exposed to the air side (Figure 1i). With the increase of solar intensity from 0.2 sun to 1.0 sun, the SPCM reached a maximum temperature of $\approx 69^\circ\text{C}$.

To demonstrate the advantage of the asymmetric structure, the homogenous composite of candle soot and PDMS membrane was fabricated via in situ coating approach (Figure 2a). The obtained composite showed a homogenous structure without hierarchically interlocked layer, which also resulted in a prominently reduced WCA value of 106° (Figure 2b). Note that the candle soot was almost covered by the PDMS layer, which could severely reduce the solar-to-thermal conversion. As shown in Figure 2c, the in situ composite experienced a gradual increase of the generated temperature under a series of solar intensity from 0.2 to 1 sun, showing a maximum value of $\approx 55^\circ\text{C}$. However, the SPCM with partially exposed candle soot could reach up to an equilibrium temperature of $\approx 73^\circ\text{C}$ (Figure 2d). Although the in situ composite also demonstrated the capability of high absorption and emissivity, the physically coated PDMS layer could result in unfavorable thermal transmission and corresponding reduced temperature (Figure S24, Supporting Information). Specifically, it was clearly observed that the temperature on the PDMS side of the SPCM was higher than that of the candle soot side under a series of solar intensity from 0.2 to 1 sun (Figure 2e). Besides, pure PDMS film with the same thickness was also prepared in our experiment. As displayed in Figure 2f, the heating rate of SPCM was remarkably higher than that of pure PDMS film under low solar intensity from 0.2 to 0.8 sun. Furthermore, the temperature difference between film surface and the inner space gradually decreased with the increase of solar intensity (Figure S25, Supporting Information). As a result, the advantage of efficient thermal management of SPCM at low solar intensity was demonstrated, enabling $\approx 88.23\%$ thermal management efficiency even under 0.2 sun ($\varphi = T_{\text{mana}} / T_{\text{film}} * 100\%$).

To further explore the working mechanism of the SPCM, a schematic of SPCM was illustrated in Figure 2g. In our system the thermal management process of SPCM was divided into three steps: first, sunlight penetrated into the transparent PDMS layer and further was absorbed by candle soot layer for efficient solar-to-thermal conversion. Owing to the interlocked structure for effective thermal transfer, the heat from the candle soot side was transmitted to the PDMS side. Thanks to the PDMS had low specific heat capacity, heat transferred from the candle soot side was further accumulated and stored, resulting in a slightly higher temperature of the PDMS side than that of the candle soot side. Meanwhile, the generated heat could enable effective thermal emission to heat the inner space. To further investigate the working mechanism, the theoretical analysis based on the transient heat transfer model by COMSOL software was conducted in our system (Figure 2h, detailed explanation in Section 1). The simulated model was composed of photothermal candle soot layer and transparent PDMS layer, which was also endowed with intrinsic factors of thermal conductivity and absorptivity. When the sunlight was applied to the model, the bottom layer of candle soot could experience a sharp increase of temperature after 1.5 s. With the increase of irradiation time, the temperature of the top layer of PDMS showed a higher value due to the thermal accumulation inside the PDMS network. As a result, the balanced temperature of the PDMS layer and candle soot layer were ≈ 76 and 72.6°C , respectively (Figure 2i). Based on the aforementioned analysis, the theoretical simulation was consistent with our experimental result.

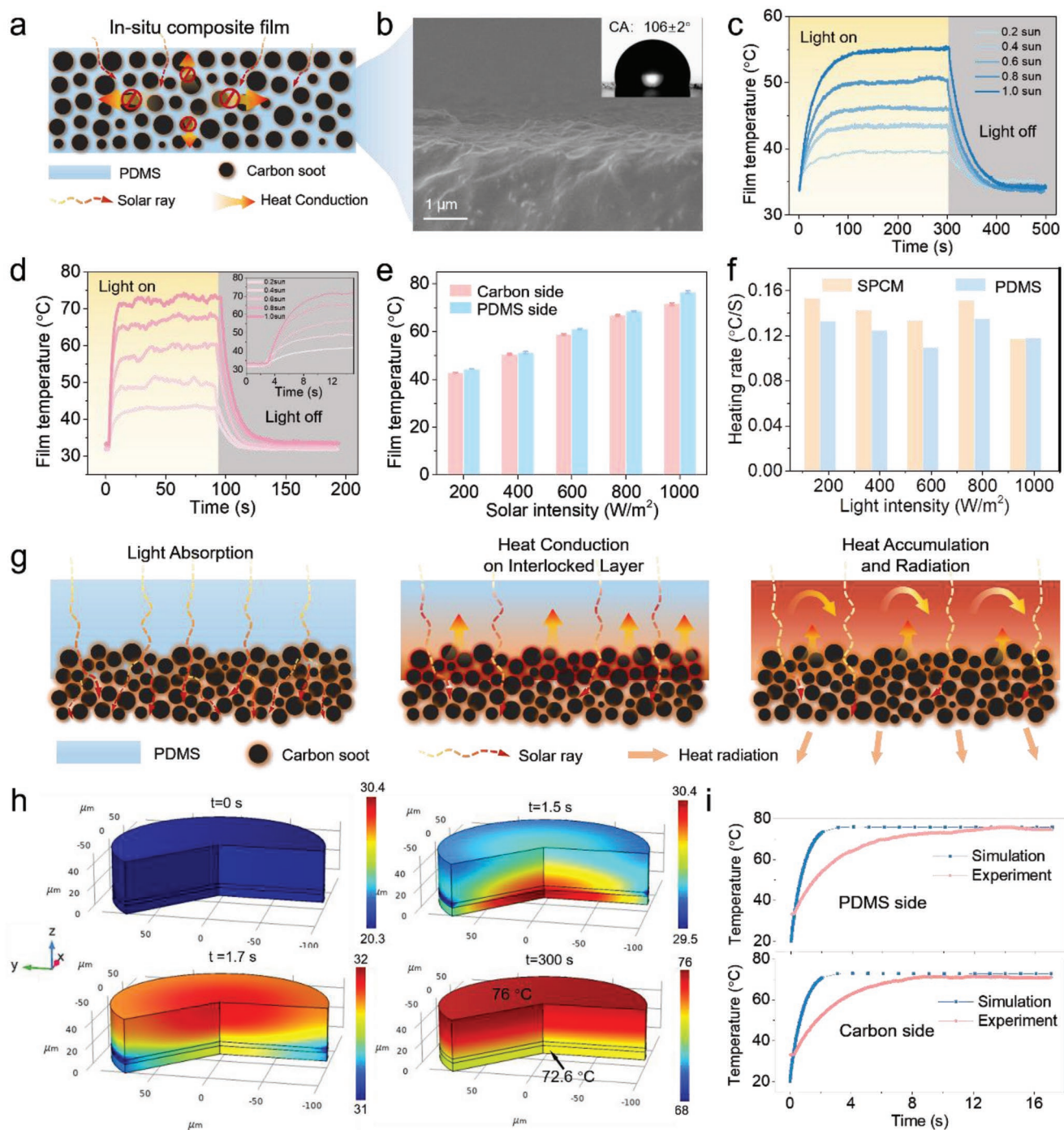


Figure 2. Photothermal conversion and working principle of SPCM. Schematic diagram of heat conduction of in situ coated composite film a) and SEM image of cross section b), inset: the image of contact angle (CA) $\approx 106^\circ$. c) Temperature-time curves of in situ composite film under 0.2 sun–1.0 sun. d) Temperature-time curves of SPCM with interlocking layer under 0.2 sun–1.0 sun. e) The infrared temperature on both sides of SPCM at different solar intensities of 200–1000 W m^{-2} . f) Comparison of heating rates between SPCM and pure PDMS under 200–1000 W m^{-2} . g) Working mechanism of SPCM. h) Theoretical simulation analysis and temperature distribution based on steady-state heat transfer models (diameter: 100 μm). i) Comparison of simulated and experimental results of SPCM temperature.

Specifically, to maintain a stable solar-to-thermal performance, the water-repellant capability of the SPCM was further investigated. As displayed in Figure 3a, with the deposition time of candle soot increasing from 30 to 300 s, the WCA of

SPCM could maintain a value of above 156° . Note that thickness of PDMS layer has little effect on WCA value of SPCM (Figure S26, Supporting Information). To evaluate the superhydrophobic stability of SPCM, it was mechanically rubbed

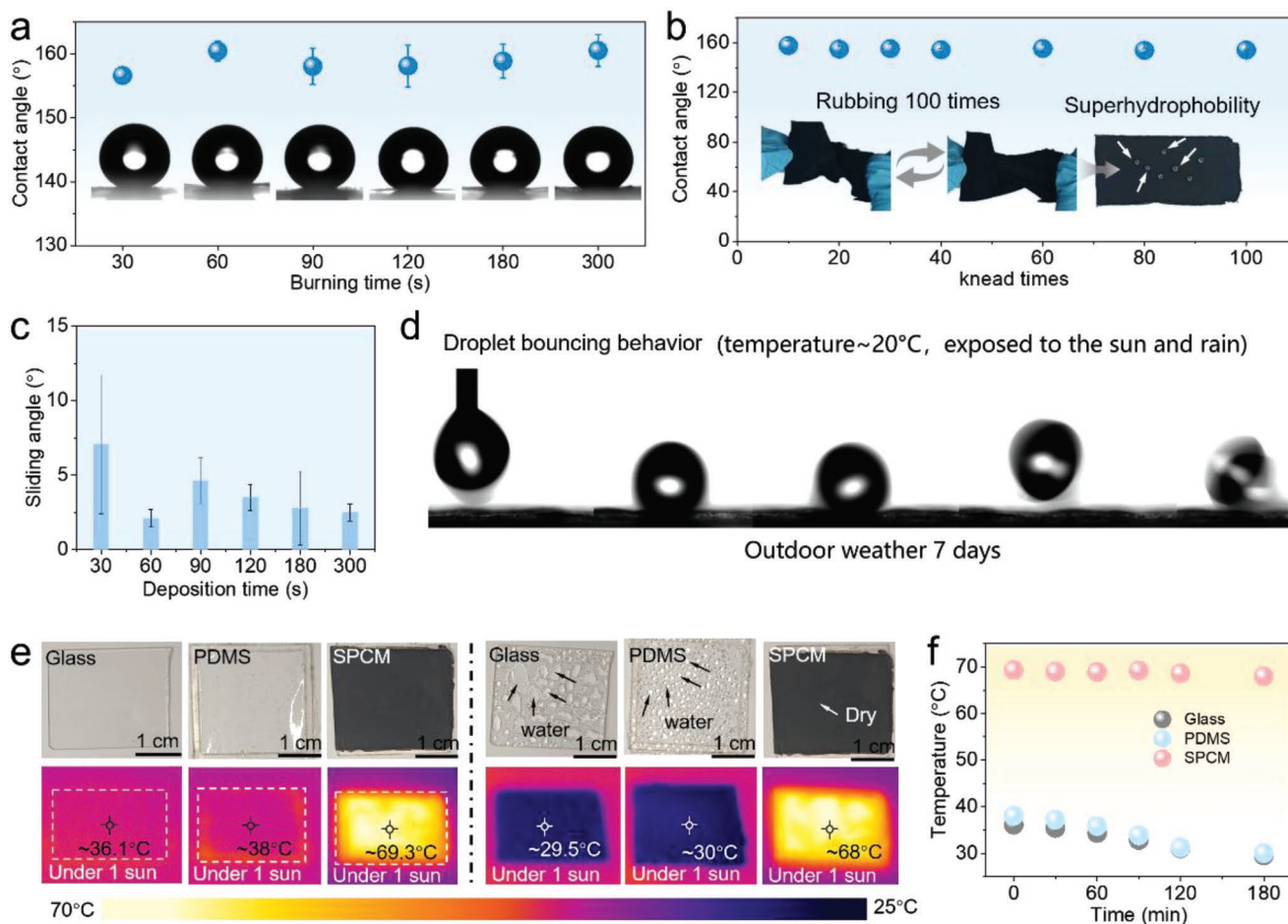


Figure 3. Superhydrophobic properties of SPCM. a) Water contact angle and images of different deposition time of candle soot (the sample size: $\approx 4 \text{ cm} \times 2 \text{ cm}$, test number: $n = 6$). b) Water contact angle of SPCM after rubbing 10, 20, 30, 40, 60, 80 and 100 times respectively (test number: $n = 7$). c) The sliding angle (SA) of SPCM under different deposition time of candle soot (the sample size: $\approx 4 \text{ cm} \times 2 \text{ cm}$, test number: $n = 6$). d) Droplet bounce behavior after SPCM was exposed outdoors at 20°C for 7 days. e) Temperature changes and infrared images before and after water droplet condensation (room temperature: $\approx 28^\circ \text{C}$). f) Temperature – time curves of glass, PDMS and SPCM in evaporative water condensation experiments (the sample size: $\approx 2.5 \text{ cm} \times 2.5 \text{ cm}$, test number: $n = 3$). Five different positions were measured for each sample, water droplets = $3 \mu\text{L}$.

for 10, 20, 30, 40, 60, 80 and 100 times, respectively. As a result, the WCA and SA value of SPCM only experienced a slight decrease and increase respectively after 100 cycles of rubbing (Figure 3b; Figure S27, Supporting Information). In addition, the SA under different deposition time of candle soot was also measured, showing a value of $\approx 2.5^\circ$ at 5 min (Figure 3c). Furthermore, the durability of SPCM was conducted in an outdoor environment for 7 days. As displayed in Figure 3d, the bouncing behavior of water droplets was still maintained. Besides, SPCM demonstrated favorable self-cleaning capability. In our system, the dust on the surface of SPCM could be easily removed by the rolling water droplets and the temperature of SPCM could maintain $\approx 72^\circ \text{C}$ under 1 sun (Figure S28, Supporting Information).

Benefitted from the favorable superhydrophobic feature of SPCM, the stability of solar-to-thermal performance was further investigated. As shown in Figure S29 (Supporting Information), SPCM, glass and PDMS were used as the roofs of the sealed containers, in which there was appropriate water to simulate the environment of green house. When the sunlight was

applied to the aforementioned three models, the equilibrium temperature values before water condensation were 36.1, 38, and 69.3°C , respectively (Figure 3e). With the increase of irradiation time for 3 h, there were remarkable water droplets condensation on the surface of PDMS and glass roofs. However, there was no water droplet condensed on the surface of SPCM. To further explore the reason, the film was placed on top of a closed container containing $\approx 40^\circ \text{C}$ hot water (Figure S30a,b, Supporting Information). In the absence of sunlight, the temperature-time curve showed that PVC had a larger temperature difference than SPCM (Figure S30c, Supporting Information). In addition, it is clearly observed from Figure S31 (Supporting Information) that there is significant condensation of water droplets on the PVC surface, while there is no water infiltration on the SPCM surface in the absence of sunlight, indicating that the superhydrophobic property of SPCM can inhibit the condensation of water droplets. Therefore, compared with glass and PDMS, the temperature of SPCM could still maintain a stable value of $\approx 68^\circ \text{C}$ under 1 sun (Figure 3f). Significantly, the effective combination of superhydrophobic and photothermal

features has provided an alternative pathway of the realization of durable solar-to-thermal materials and related devices.

Based on the favorable superhydrophobic and photothermal feature of the SPCM, as a demo, it was employed as a solar-to-thermal roof for effective thermal management device. In our system, pure transparent glass and PDMS were alternatively selected as the control samples. Since the glass and PDMS were both featured with high transmittance and emissivity, the penetrated sunlight could heat the air inside the room models (Figure 4a–d; Figures S32,S33, Supporting Information). However, it could effectively decrease the heat dissipation due to the pure PDMS with low thermal conductivity. In addition, superior

to the glass and PDMS samples, the SPCM was characterized of high solar-to-thermal conversion and high emissivity, which could provide remarkably enhanced temperature and further heat the air via the thermal conduction, convection and radiation. In our system, SPCM, glass and PDMS were used as roofs and glass was selected as wall (Figure 4e). To simulate the conventional solar intensity, the solar intensity of 0.4 sun was employed in our experiment. As shown in Figure 4f, the temperature of SPCM could reach up to $\approx 50\text{ }^{\circ}\text{C}$, which was $\approx 15\text{ }^{\circ}\text{C}$ higher than that of PDMS and glass samples. More importantly, with the increase of irradiation time, the temperature of PDMS and glass samples first increased and subsequently decreased.

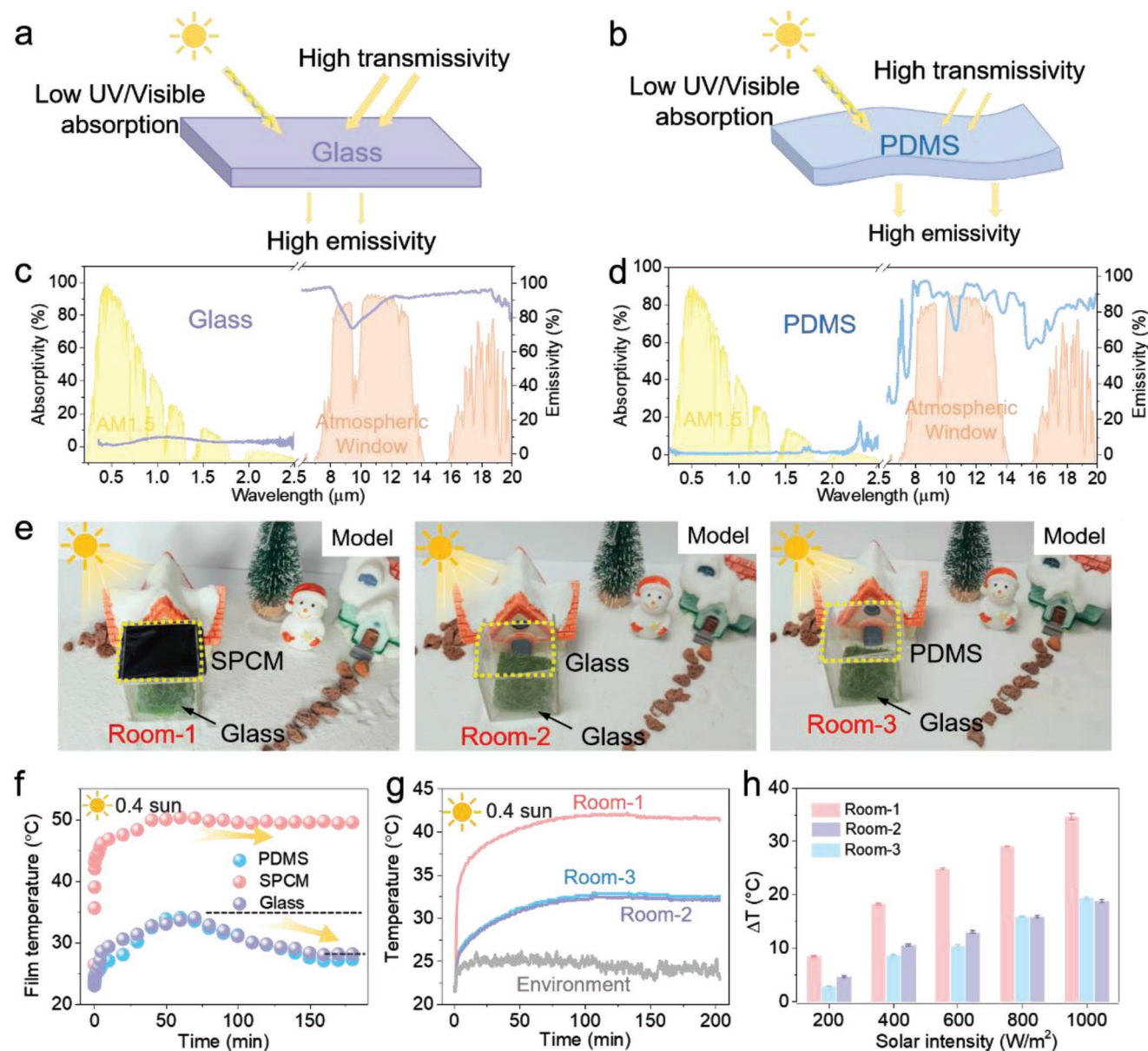


Figure 4. SPCM for greenhouse thermal management application. Diagram of the working mechanism of glass a) and PDMS film b). Solar absorptivity and thermal emissivity spectra of glass c) and PDMS d). e) Greenhouse thermal management model of SPCM (Room-1), Glass (Room-2) and PDMS (Room-3) (glass around) (the sample size: $\approx 2.5\text{ cm} \times 2.5\text{ cm}$, test number: $n = 3$). f) Real-time film temperature-time curves for SPCM, Glass, and PDMS (under 0.4 sun). g) Real-time greenhouse thermal management temperature-time curves for SPCM, Glass and PDMS (under 0.4 sun). h) The temperature difference between Room-1, Room-2, Room-3 and the environment under different levels of sunlight ($200\text{--}1000\text{ W m}^{-2}$).

This phenomenon resulted from the water droplets condensed on the roof under the sealed system, which may further decrease the balanced temperature of PDMS and glass samples. Owing to the superhydrophobic feature, SPCM could still maintain a stable equilibrium temperature. Moreover, the surface and section EDS of SPCM show that candle soot has excellent dispersion in PDMS, which further indicated that SPCM had stable and uniform indoor thermal management (Figure S34, Supporting Information). In addition, the real-time temperature inside the room models was also monitored in Figure 4g. The result showed that the balanced temperature of room-1 was ≈ 10 °C higher than that of room-2 and room-3, indicating that the excellent super-hydrophobicity of the SPCM enables it to be continuously heated and maintain the desired temperature stability in the room. Also, real-time temperature-time curves of SPCM, glass and PDMS and corresponding environment under 0.2, 0.6, 0.8, and 1.0 sun was conducted in Figure S35 (Supporting Information). Furthermore, the cyclic stability was also investigated in our system. As shown in Figure S36 (Supporting Information), SPCM-based solar heater could enable a favorable cyclic stability, demonstrating enhanced film temperature of ≈ 28 °C higher than that of the ambient condition under 0.6 sun. The result indicated that SPCM enabled favorable solar-to-thermal conversion performance.

Specifically, the COMSOL theoretical analysis was also performed based on a steady-state heat transfer (Figure S37, Supplement section 2 for detail). The balanced temperature of SPCM model could experience a remarkably enhanced temperature under 1.0 sun. Based on the aforementioned analysis, the theoretical simulation was consistent with our experimental result.

In order to evaluate the thermal management capability, the temperature difference (ΔT) between the temperature of room-1, room-2, room-3 and the ambient temperature under a series of solar intensities ($200\text{--}1000\text{ W m}^{-2}$) was calculated in Figure 4h. The temperature inside room 1 was ≈ 9 °C higher than the ambient temperature even under low solar intensity of 0.2 sun. The highly improved temperature difference illustrates that the SPCM exhibits the potentials in the application of energy-free thermal management compared with the traditional heating methods (such as air conditioning, hot air, etc.).

Based on superior space temperature regulation ability, the SPCM can maintain a temperature gradient between its surface and indoor in the working modes. As a proof-of-concept, the outdoor bean sprout simulation was designed to work on a sunny winter day. Four insulated foam boxes were used as seed germination containers, and each group contained eight bean seedlings. And commercial black polyvinyl chloride (PVC) membrane, PDMS, SPCM and blank control were introduced into the four boxes to form artificial greenhouse, individually (Figure 5a). The surface temperature of the four systems at 12:00 AM and 5:00 PM in one day was first measured. As shown in Figure 5b, SPCM could maintain higher temperature throughout the day. Noted that the high temperature of the blank sample at 12:00 AM may derive from the small specific heat capacity of sand and stone. On the other hand, the surface temperature of the PDMS and PVC samples experienced remarkable decrease after continuous solar irradiation, which resulted from the cooling effect of the condensed water drop-

lets under sealed systems. Furthermore, the condensed water could be easily observed in the samples of PVC and PDMS (Figure 5c). However, there was no water droplet observed on the inner surface of the SPCM owing to its favorable superhydrophobic feature. In addition, we also measured the stability of the SPCM-enabled solar heater after one night. When the samples were irradiated again on the second day, only SPCM could maintain a high temperature. The other two samples with PVC and PDMS showed severely reduced temperatures attributed to the condensed water on the surfaces of membranes (Figure 5d,e).

In one day, the real-time indoor temperature curves of the four systems were also monitored in Figure 5f. The results found that the temperature of SPCM always maintained higher temperature than that of the other three samples. The inner temperature of SPCM system was 4, 6, and 12 °C higher than that of PVC, PDMS and the environment at 12:00 AM. Although the commercial PVC was also endowed with black color, it had low absorption and poor emissivity (Figure S38, Supporting Information). Therefore, SPCM sample could demonstrate enhanced surface temperature and corresponding temperature differentiation with the environment. In addition, the real-time temperature difference between SPCM and related solar intensity were monitored in Figure 5g. It was observed that the temperature difference could maintain above 4 °C even at night due to its stable insulation performance. To further demonstrate the environmental adaptability of SPCM, the ice resistance of Glass, PDMS, PVC and SPCM film was also explored (Figure S39, Supporting Information). Even under low solar intensity (0.2 sun), SPCM could still exhibit favorable capability of ice resistance owing to the good superhydrophobic and photothermal performance. In addition, the superhydrophobic stability of SPCM before and after 20 cycles of melting experiments was further investigated. As shown in Figure S40 (Supporting Information), the surface morphology of SPCM almost remained unchanged and the water contact angle was higher than 150° before and after 20 times of melting, suggesting that SPCM had stable superhydrophobic properties during the melting cycle. Moreover, ice adhesion tests show that ice adhesion strength of SPCM surface increases with the increase of melting times (Figure S41, Supporting Information).

To investigate the outdoor growth of bean sprout in control groups, the number of germination sprouts was quantitatively recorded in Figure 6a. Noted that appropriate temperature is one critical factor that can remarkably boost germination sprouts. In our experiments, after 9 days, the sprout numbers of blank, PVC, SPCM and PDMS systems were 0, 5, 8, 4, respectively, indicating that SPCM-enabled system can effectively boost the germination rate of bean sprouts. For the blank sample, the large temperature difference between day and night resulted in a 0% germination rate of bean sprouts. On the other hand, for the samples of black PVC and transparent PDMS, there was almost no effect on the germination rate of bean sprouts. As previously reported by Fakir et al., the germination of bean sprouts was not prominently affected by light under certain temperature.^[59–61] This result was also consistent with the reported phenomenon. Since 8 seeds were added into the four control samples, only SPCM group could reach germination rate of 100% on the 9th day first (Figure 6b). However,

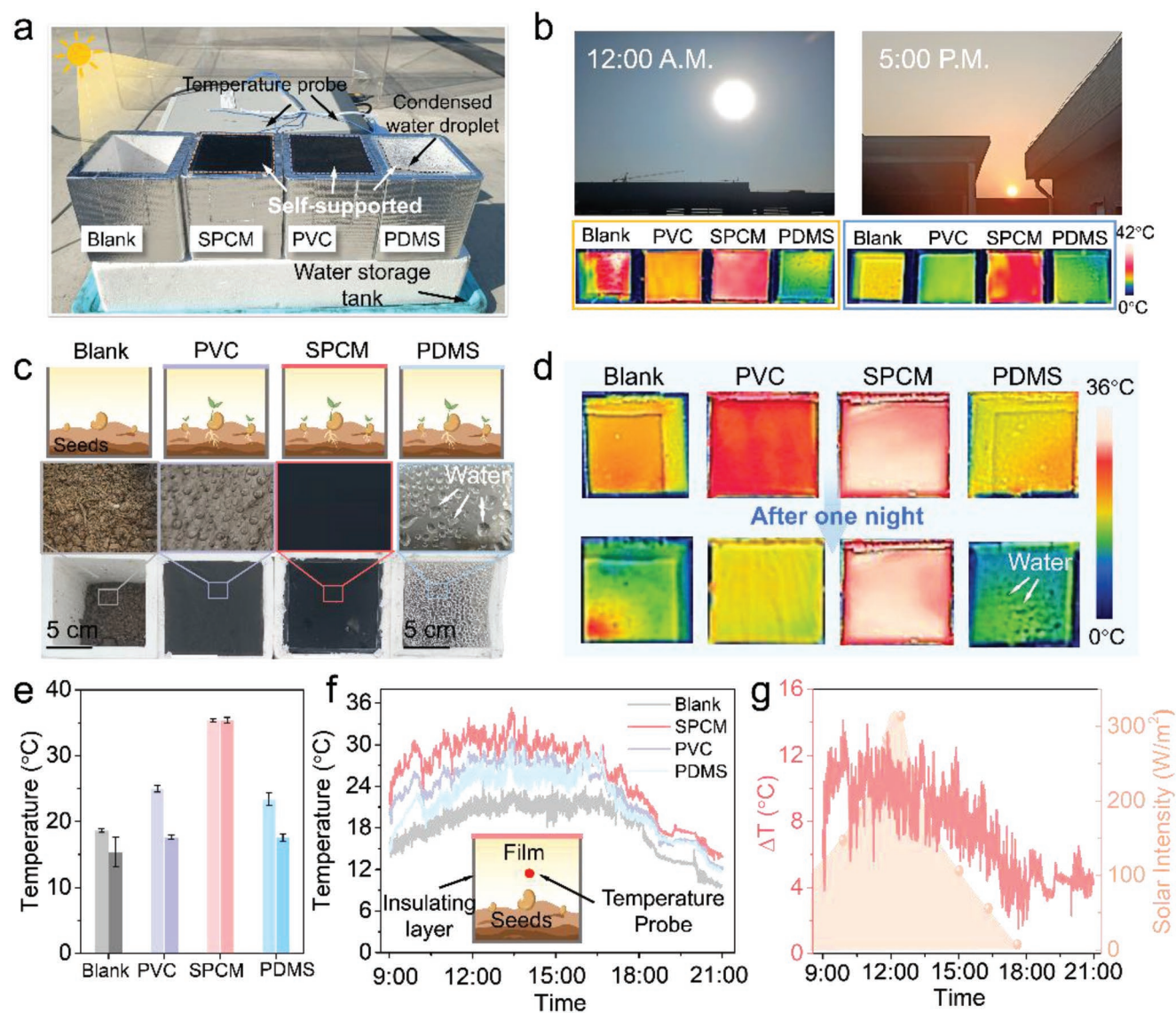


Figure 5. Outdoor experiment with SPCM. a) Digital images of experiment in an outdoor environment on a sunny day in winter (Nov. 10th, 2021, east longitude: $\approx 121^\circ$; northern latitude: $\approx 29^\circ$). b) Real-time weather digital images and thermal infrared images of PVC, SPCM, PDMS and blank control group at 12:00 A.M. and 5:00 P.M., respectively. c) Digital images of PVC, SPCM, PDMS and blank group after one day in sunlight. Thermal infrared images (d) and film temperature diagram (e) of PVC, SPCM, PDMS and blank groups of uncondensed water droplets and one day later condensed water droplets. f) The real-time indoor temperature of PVC, SPCM, PDMS and blank control group on the sunny day (The ambient temperature was consistent with that of the blank control group). g) The real-time temperature difference between SPCM thermal management temperature and the environment in the outdoor experiment and the solar intensity at that time. (all the sample size: $\approx 10\text{ cm} \times 10\text{ cm}$, test number: $n = 4$, the film temperature is measured by an infrared detector, and a thermocouple records the indoor thermal management temperature of each sample in real time)

it was clearly observed that there were more weeds in PDMS and PVC samples than that in SPCM one. The phenomenon may derive from the fact that weeds need enough sunlight for further growth. In conclusion, it can be analyzed that SPCM displays an appropriate and wide application prospect in the growth of shade-loving crops and the germination of seeds.

To further evidence the aforementioned result, we also repeated the whole process by using three parallel groups (Figure S42, Supporting Information). As shown in Figure 6c and Figure S43 (Supporting Information), SPCM-enabled system represented the most sprouts on the fourth day. And it

had higher germination rate than that of the other three control samples. Compared with the commercial black PVC system, the SPCM one demonstrated a remarkable increase of the germination rate of $\approx 30\%$. Therefore, SPCM-enabled system is expected to provide efficient and continuous thermal energy supply for the agricultural production improvement. However, compared with cost and scalability of the commercial PVC membrane, SPCM materials are in their infancy. Although the SPCM has showed better photothermal performance than that of the commercial PVC membrane, it is still confronted with a series of challenges, such as technical maturity and cost. Specifically, as

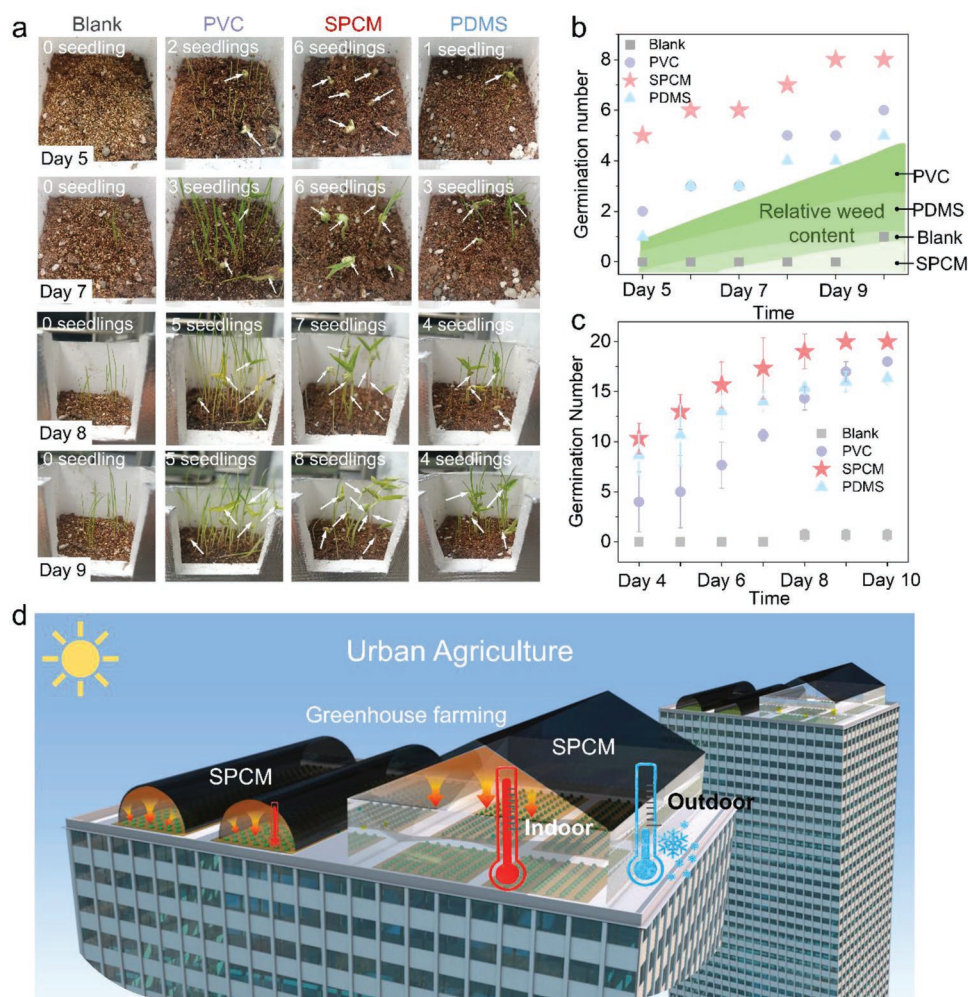


Figure 6. Application of SPCM in urban agriculture. a) Schematic diagram of bean sprouts real-time growth on day 5 to day 9 of PVC, SPCM, PDMS and blank group (all the sample size: $\approx 10 \text{ cm} \times 10 \text{ cm}$, test number: $n = 4$). b) Schematic diagram of real-time sprout number and relative weed content of PVC, SPCM, PDMS and blank group. c) The number of real-time bean sprouts of PVC, SPCM, PDMS and blank group in the three groups of repeated experiments (all the sample size: $\approx 10 \text{ cm} \times 10 \text{ cm}$, test number: $n = 12$). d) Application model and prospect of SPCM in urban agriculture.

a demo, the potential application of urban agriculture was carefully devised in Figure 6d, which could take full advantage of the space and solar energy for continuous and stable thermal management.

3. Conclusion

In summary, we have proposed a Janus membrane with hierarchically nanostructured candle soot partially embedded in PDMS elastomer in a simple, effective, and scalable way, enabling favorable superhydrophobic and photothermal properties. Also, the design principle of asymmetric structure with PDMS as the outer layer of light transmission and thermal isolation enables the efficient thermal utilization with lower heat dissipation. Based on these advantages, the Janus membrane can function as a water-repellent management device to continuously heat the closed area, in which no liquid water can be condensed on the membrane and the generated temperature can maintain

a stable value. Furthermore, the attempt on the heating membrane for the growth of bean sprouts has been also conducted. Superior to the commercial one, the proposed membrane can resist the condensation of water, enable enhanced temperature and maintain stable thermal supply under the closed system for remarkable improvement of the germination rate. As a result, the design of asymmetric structure of the superhydrophobic and photothermal membrane is expected to be a new pathway for developing environmentally stable thermal management devices, demonstrating promising potentials in low-carbon house system and new-generation of urban agriculture.

4. Experimental Section

Materials: Candle soot was deposited by the burning of cheap and common commercial white candles. Glass slide (thick, $\approx 2 \text{ mm}$; size, $10 \times 10 \text{ cm}^2$) was rinsed with deionized water and ethanol, then dried with a nonwoven cloth, and used as a transfer substrate. PDMS film was fabricated from Sylgard 184 (the ratio of base-to-curing was 10:1). Before

film formation, the PDMS and corresponding cross-linker were diluted using n-heptane with a volume of 25 mL. General chemicals in chemical reagent grade were used as received from Sinopharm Chemical Reagent.

Fabrication of Superhydrophobic Photothermal SPCM: First, the clean glass slide was held above the candle flame and a thick layer of a multi-level structure of candle soot was deposited after 5 min. Candle soot was cooled in the air for half an hour to make it more stable. 25 mL of the mixture of 16 wt% PDMS in n-heptane was sprayed onto the air/water interface to achieve a homogenous layer, followed by PDMS procuring process (at 65 °C for 45 min) to form a uniform semi-polymerized PDMS film. At this time, most of the solvent of PDMS prepolymer at the water/air interface was volatilized and the PDMS on the air side still had fluidity due to the temperature difference between the water side and the air side. Then, the semi-polymerized PDMS film was transferred from the air side by a glass slide deposited with candle soot. It was worth noting that the degree of film formation should be measured with forceps around before transfer. Finally, the transferred SPCM was further cured at 80 °C for 2 h, and the substrate was directly stripped to obtain SPCM with interlocked structure.

Thermal Management Measurements: The cuboid with the size of 8 cm³, no lid and hollow transparent glass was covered with photothermal SPCM. Two temperature probes were placed in the center of the cube (at different horizontal positions) to monitor the temperature changes in the internal space in real-time. During measurement, the SPCM was sealed with adiabatic tape to ensure a closed system. Water vapor condensation experiment: 2 mL water was added to an adiabatic cube model and placed under 1 sun for 3 h. After complete cooling, water vapor condensed when it met the top glass and PDMS, while SPCM had no condensation of water droplets due to its excellent superhydrophobic properties.

Outdoor Farm Simulation Experiment: The insulated foam box (size : 10 × 10 × 15 cm³) was perforated at the bottom and side to ensure oxygen for plants. Superabsorbent cotton ropes were drained from the bottom to the inside to maintain water supply to the soil. Commercial planting nutrient soil was added to half of the incubator, mung bean seeds were placed on the surface of the nutrient soil. After spraying water, a layer of nutrient soil with a thickness of 0.5 cm was covered. The temperature probe was placed 1 cm above the soil and sealed around the film with insulation tape. The sunlight intensity and temperature in the outdoor bean sprout experiment (Ningbo in South China: East longitude ≈121° and North latitude ≈29°) were recorded from 9 o'clock to 21 o'clock (Nov. 10th, 2021).

Characterization: Field emission scanning electron microscope (FE-SEM) with a FE scanning electron microanalyzer (Hitachi-S4800, 4 kV) was used to observe the morphologies and microstructures of SPCM with interlocking layer and without interlocking layer. Intelligent Fourier infrared spectrometer (FTIR) infrared was used to characterize the infrared emission spectra of SPCM, glass, PDMS and PVC at 2.5–20 μm band (Cary660+620). The absorption spectra of samples were performed using an UV–vis–NIR spectrophotometer equipped with an integrating sphere (Lambda 950). Greenhouse thermal management was carried out under the irradiation of Solar Simulator (HM-Xe500W). IR thermal images and the corresponding film temperatures were captured using the IR thermal camera (Optris pi 400). The stress-strain curve was measured by using the universal material testing machine (Zwick Z1.0). Temperature detector (JK4000) was used for thermal management space temperature acquisition in indoor and outdoor. In the outdoor farm experiment, IR thermal images were captured by Handheld thermographic imager (FLIR-E6390, Estonia). The wettability of the membrane was performed on the contact angle measuring instrument (OCA20, America) at room temperature. More than three different positions were measured for each sample (water droplets ≈ 3 μL). The ice adhesion shear strength was measured with a force transducer (ZTS-500N), and the sample was frozen at –20 °C for 2 h to ensure that water froze completely. The ice adhesion strengths were averaged over at least three measurements. The surface roughness of the SPCM was measured by using the scanning probe microscope (Dimension ICON SPM). The photos in this article were taken with Xiaomi K30 smartphone.

Statistical Analysis: The experimental data of temperature–time curve was not pre-processed. The temperature at PDMS side and Carbon soot side were tested by thermocouple on both sides at the same time, and the error bars of experimental data were presented with mean ± standard deviation (SD). The sample size for optical characterization was 3 × 3 cm. The experimental data of contact angles and sliding angles were tested at least three locations and presented with mean ± standard deviation (water drop = 3 μL). The software of Excel was employed to conduct one-way analysis of variance (one-way ANOVA) and the difference among samples was considered to be important when the calculated p value was lower than 0.05.

Supporting Information

Supporting Information is available from the Wiley Online Library or from the author.

Acknowledgements

Thanks for the assist of Prof. Li Tong of the Marine Laboratory of Ningbo Institute of Materials Technology and Engineering, Chinese Academy of Sciences that provided device of the ice adhesion test. This research was supported by the Natural Science Foundation of China (52073295), the National Key Research and Development Program of China (2022YFC2805204), Ningbo Science and Technology Bureau (2021Z127), the Sino-German Mobility Program (M-0424), Ningbo Public Welfare Science and Technology Plan Project (2021S150), Key Research Program of Frontier Sciences, Chinese Academy of Sciences (QYZDB-SSWSLH036), Bureau of International Cooperation, Chinese Academy of Sciences (174433KYSB20170061), and K. C. Wong Education Foundation (CJTD-2019-13).

Conflict of Interest

The authors declare no conflict of interest.

Author Contributions

P.X. and S.L. conceived the idea. S.L. designed the experiments and performed the material preparation and characterization. S.L. performed the modelling and the outdoor experiments work with the help of W.Y., J.G. and C.Z. P.X. helped with writing the manuscript. T.C. and S.K. supervised the project and provided financial support. All the authors provided discussion and comments.

Data Availability Statement

The data that support the findings of this study are available on request from the corresponding author. The data are not publicly available due to privacy or ethical restrictions.

Keywords

nanostructured membranes, self-supported and self-adaptive, superhydrophobic and photothermal, thermal management, urban agriculture

Received: August 20, 2022

Revised: January 7, 2023

Published online:

